Design and Implementation of an Ultralow-Power ECG Patch and Smart Cloud-Based Platform

SUBMISSION DATE / POSTED DATE

12-11-2021 / 21-04-2022

CITATION

Baraeinejad, Bardia; Fallah Shayan, Masood; Vazifeh, Amir Reza; Rashidi, Diba; Saberi Hamedani, Mohammad; Tavolinejad, Hamed; et al. (2021): Design and Implementation of an Ultralow-Power ECG Patch and Smart Cloud-Based Platform. TechRxiv. Preprint. https://doi.org/10.36227/techrxiv.17003401.v6

DOI

10.36227/techrxiv.17003401.v6

Design and Implementation of an Ultralow-Power ECG Patch and Smart Cloud-Based Platform

Bardia Baraeinejad, Masood Fallah Shayan, Amir Reza Vazifeh, Diba Rashidi, Mohammad Saberi Hamedani, Hamed Tavolinejad, Pouya Gorji, Parsa Razmara, Kiarash Vaziri, Daryoosh Vashaee, Mohammad Fakharzadeh, *Senior Member, IEEE*

Abstract

This paper reports the development of a new smart ECG monitoring system, consisting of the related hardware, firmware, and IoT-based web service for AI assisted arrhythmia detection and a complementary Android application for data streaming.

The hardware aspect of this research proposes an ultra-low power patch sampling ECG data at 256 samples/s with 16-bit resolution. The battery life of the device is two weeks per charging, which alongside the flexible and slim (193.7 mm × 62.4 mm × 8.6 mm) and lightweight (43 g) allows the user to continue real life activities while the real-time monitoring is being done without interruption. The power management is achieved through the usage of switching converters, ultra-low power component choice as well as intermittent usage of them through firmware optimization. A novel data encoding method is also proposed to allow compression of data and lower the runtime.

The software aspect, in addition to the web ECG analysis platform and the Android streaming and monitoring application, provides an arrhythmia detection service. The key innovations in this regard are the usage of a set of new factors in determining arrhythmia that grants higher accuracy while retaining the detection near-real-time. The arrhythmia detection algorithm shows 98.7% accuracy using Artificial Neural Network and K-Nearest Neighbors methods, and 98.1% using Decision Tree method on test data set.

***Keywords*— Arrhythmia Detection, Artificial Intelligence, Cardiovascular Diseases, Cloud Storage, Electrocardiogram (ECG), Internet of Things (IoT), Wearable Sensors**

Citation information: DOI: 10.1109/TIM.2022.3164151

B. Baraeinejad, A. Vazifeh, P. Razmara, K. Vaziri, and M. Fakharzadeh are with the Electrical Engineering Department, Sharif University of Technology, Tehran, Iran (e-mail: bardiabarai@gmail.com, amirrezavazifeh2000@hotmail.com, parsa.razm@gmail.com, kiarashvaziriblue@gmail.com, fakharzadeh@sharif.edu). M. Fallah Shayan is with the Management and Accounting Department, Shahid Beheshti University, Tehran, Iran (e-mail: masood.fsh@gmail.com). D. Rashidi is with the Mathematics Department, Alzahra University, Tehran, Iran (e-mail: dibra.rashidi@gmail.com). M. Saberi Hamedani is with the School of Medicine, Shahid Beheshti University of Medical Sciences, Tehran, Iran (e-mail: m.saberihamedani@gmail.com). H. Tavolinejad, is with Department of Cardiac Electrophysiology, Tehran Heart Center, Cardiovascular Diseases Research Institute, Tehran University of Medical Sciences, Tehran, Iran (e-mail: h.tavoli733@gmail.com). P. Gorji is with the Literature and Language Department of Tehran Azad University, North Branch, Tehran, Iran (e-mail: pgxiii@gmail.com). D. Vashaee is with the Electrical and Computer Engineering Department, North Carolina State University, Raleigh, USA (e-mail: dvashae@ncsu.edu).

I. Introduction

Cardiovascular diseases (CVD) are the leading cause of death, estimated in 2019 to cause 18.6 million deaths per year worldwide [1], while 90% of such diseases are preventable [2]. Among them, cardiac arrhythmia is a common condition. Cardiac arrhythmia and fast heart beatings may lead to symptoms such as dizziness, pounding, shortness of breath, and forceful extra heartbeats [3]. These symptoms are often accompanied by chest pain or discomfort, diaphoresis, neck fullness, or vasovagal type of response with syncope, diaphoresis, or nausea in case of tachycardia [3]. On the other hand, all types of arrhythmia may be asymptomatic [3]. Asymptomatic cardiac arrhythmia may happen so sporadically that only through extensive ECG monitoring can it be detected [4]. The rarity of such cases should not lead to underestimating their importance, as they can lead to syncope, cardiac arrest, or sudden death. However, accessibility is a major issue regarding CVD monitoring – not every artifact is expected to occur continuously or during the clinical setting of recording ECG signals [5]. Moreover, clinical ECG devices utilize several electrodes running through multiple cables, which can be challenging to set correctly by non-clinicians outside the health care facilities. On the other hand, limited Holter monitoring, four days and below, is proven to be insufficient in detecting sporadic arrhythmias. Due to limited battery life, the current Holter monitor devices do not allow extended monitoring periods with high resolution (Table II). Recent research has proven the efficacy of monitoring through single-lead ECG patches as an alternative to Holter monitoring. In a clinical study, 7-day monitoring with a single-lead ECG patch yielded more accurate results than typical 24-hour Holter monitoring [6], and another 2021 study [7] showed a 40.5% rise in arrhythmia detection rate in 14-day monitoring than lower durations. In cases such as cerebral ischemic events, a minimum of 7-day monitoring is required to detect atrial fibrillation [8], which could be lifesaving.

In 2020 and 2021, due to the health concerns regarding the COVID-19 pandemic, visiting clinics and hospitals for extended periods partially lost its feasibility, calling for alternative methods of monitoring ECG accurately at home and using telemetry for patient-doctor communication. Furthermore, ECG is proven to be a helpful measure for cardiovascular involvement in COVID-19 patients [9]. However, the utility of such devices is often overshadowed by existing hardware requiring the involvement of an independent analysis facility. Earlier efforts to create online and smartphone-based platforms that have been made are either rudimentary and outdated or lack the required detection capabilities compared to facility-based detection processes [10, Table II].

This article details our endeavor to design and manufacture a device and software that allows non-stop monitoring of

ECG signals via the Internet and the arrhythmia detection algorithm assisting in diagnosis. A variety of challenges were mentioned in different studies and this research project attempted to address them [11]. The device described is a power-efficient, ergonomic, portable, single-lead ECG monitoring patch, connectable to a smartphone via Bluetooth Low Energy, and accommodating local storage for a microSD card. The choice of components was focused firstly on efficient power consumption, to allow long term recording of ECG. The novel encoding format proposed allows highly compressed data to be sent over to smartphone and the analysis server easily via BLE, facilitating telemetry and allowing monitoring of ECG data on all ranges of Android devices with ease. Ease of use for with no prior training for patients was a major concept in regard to body design. The highly flexible design allows uninterrupted physical activity for real-time, nonstop monitoring. Furthermore, due to the financial efficiency of ECG patch monitoring devices over implanted looper recorders [12], the power management was aimed at allowing non-stop monitoring. The software aspect, including the DSP-based noise filtering, AI-assisted arrhythmia detection, patient profiling, the web service, and smartphone application that enables device-phone connection, real-time signal viewing, data collection, and storage. A novel aspect of the software section includes designing low runtime methods for real time diagnosis through usage of less commonly used factors in determining arrhythmic beats.

This paper is organized as follows. Section I presents the design and manufacturing of the hardware. Section II presents the software design aspects.

II. Hardware Design

A. Hardware Overview

Our objective is to introduce a lightweight, user-friendly, ultra-low-power alternative that can collect desired data, process it, store it, and send it to an Android device via a BLE, which can yield overall better results in terms of accuracy, resolution, sample rate and battery life than the current commercial devices.

B. Block Diagram and Explanation of Each Part

As shown in Fig. 1, the block diagram of the device includes an ARM Cortex M4F processor and multiple peripherals, including Bluetooth Low Energy 5 [13]. Moreover, the diagram shows a USB type C connected to a LiPo battery charger (for battery charging) [14], a microSD card connector (for the insertion of external memory and further data storage), a level translator (for communication between microSD card connector and MCU) [15], two pushbuttons (to turn the device on/off and to start Bluetooth advertising), a single-lead ECG Analog Front-End (which uses two electrodes and amplifies the differential voltage also known as ECG AFE) [16], an accelerometer (for motion detection of the user) [17], three LEDs and a buzzer (to indicate notifications), and two DC-DC step-down converters (which supply 1.8 Volt and 3.3 Volt power from the battery to all parts) [18].

1) Sensors - ECG AFE, Accelerometer

Two sensors are integrated into the device: a single-lead ECG analog front-end (AFE) and an accelerometer. ECG AFE provides an electrocardiographic waveform through two electrodes connected via coaxial cables (shielded for noise reduction) to IPX connectors. MAX30003 was chosen for this purpose to provide a high level of configurability. The following features make this specific sensor a fitting choice.

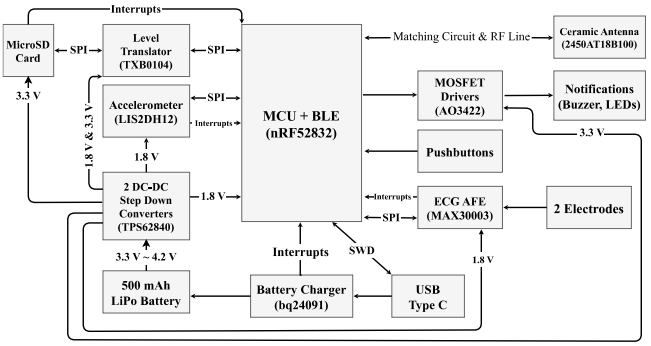

Fig. 1. Block diagram of the ECG patch hardware – The sensors, the BLE unit and the microcontroller run on 1.8V except for microSD and the drivers connected to the interface elements running on 3.3V. Two step-down converters directly connect to the 3.3~4.2V LiPo battery to power the mentioned sectors.

A lead-on/lead-off detection feature allows the microcontroller to detect sensor-body attachment to lessen power consumption. The amplifier voltage gain within the sensor is programmable, ranging from 20V/V to 160V/V. The ADC resolution is 18bits (the effective number of bits is 15.1 so we use 16 most significant bits, and the peak-to-peak noise is 5.44 µV in the present device configuration). It also has high AC dynamic range ($65mV_{P-P}$) preventing saturation. The power consumption of the ECG AFE is 180µW, according to its datasheet [16] and verified by measurement. Different research and hardware specifications were used as the basis of 256 sample/second ECG recording. Although Scher and Young [19] attributed the majority of healthy heart signals to the 0-100 Hz range, necessitating 200 sample/second recordings (according to the Nyquist theorem), several researchers [20, 21, 22] have suggested the necessity of recording higher frequencies in case of certain cardiac complications. The sample rate configuration is also determined according to the data provided in the datasheet to maximize the recorded frequencies to meet the requirements set by the mentioned research. Despite being configured to 256 samples/second, it is possible to ramp up the sampling rate to 512 samples/second without modifying the hardware if the conditions requiring higher frequencies are met.

A 3-axis accelerometer (LIS2DH12) is included to detect motion, track physical activity, and detect slips and falls. Furthermore, the data from the accelerometer enables detecting the noise caused by muscle artifacts and errors due to shakes. The said sensor works in low power mode i.e. 8 bit mode. Its power consumption is 20µW, according to its datasheet [17] and verified by measurement.

2) Power Management

A rechargeable 500 mAh lithium-ion polymer battery is used to power the circuit. Two step-down DC-DC buck converters (TPS62840) regulate the voltage to 3.3V and 1.8V. These converters are highly efficient to assist in achieving a high battery life (around 90% in the functioning voltage and current) [18]. In addition, an integrated linear battery charger (bq24091) supplied by a USB type C port is used to recharge the battery [14]. A complete cycle takes around three hours. The choice of 500 mAh battery capacity was made according to the overall current consumption of the device, i.e., 1.4 mA at 3.7 V battery voltage, enabling more than two weeks of battery life.

3) Microcontroller and Peripherals

The processing core (nRF52832) is powered by a 32-bit ARM Cortex M4F running at 64 MHz. This processor was chosen due to its low power usage and hardware capabilities. Its power consumption varies from 0.3 µA in idle mode to 58 µA/MHz when running from flash memory according to the datasheet. The microcontroller is equipped with 64 KBs of RAM and a 512 KB flash memory. SPI (Serial Peripheral Interface) is used for data transfer, with an instance for data from the sensors and another for microSD output. Serial Wire Debug (SWD) protocol was used to program this microcontroller. Two of the extra pins in the USB type C port were used for this process, one for SWDCLK and the other for SWDIO. A BLE 5 (Bluetooth Low Energy) transceiver sends data packets to and receives configurations from the connected Android device [13]. The MCU handles data encoding (further explained in *Storage* section) and BLE streaming (further explained in *Android application* section), as well as interface functions (further explained in *LEDs, Buzzer, and Pushbuttons* section).

4) Storage

A microSD card can be optionally inserted into the device to save a backup of the data collected from the sensors in a format designed to be compatible with the web application (Refer to the section on web application for further explanation). Furthermore, a level translator supplies the 3.3V needed for the microSD as opposed to the 1.8V the microcontroller runs on [15].

To simplify later analysis, the recordings are segmented into hourly files. The output is encoded into two separate files per hour. The accelerometer data is stored in the ".ACC" format and the ECG data in the ".ECG" format. The ".ACC" file stores the data from each axis in hexadecimal two's complement format (2 characters per axis, 6 characters total), compatible with the 8-bit resolution of the accelerometer module. For example, an input of $x = 20, y = -1, x_3 = -128$ is stored as "14FF80" in string format.

Delta-Sigma method has been deployed for lossless compression of the ECG data. The first sample of each hourly file is stored in its first 4 characters, in hexadecimal two's complement based on the 16-bit resolution the ECG data is recorded in. The consequent bytes store the difference of the new inputs from the initial 2 bytes, also in hexadecimal format. As an example, an input of $x_1 = -1, x_2 = 20, x_3 = 10$ would be stored as "FFFF+15-A" in string format instead of "FFFF0014000A". This can significantly decrease the file size, facilitating faster uploads to the server. Lead-on detection is marked by an "e:" in the file and lead-off is similarly marked by a "d:". Each lead-on/off event starts a new line in the file and until the lead-on/off status changes no further output regarding its status is recorded. The lead-on/off reporting is done to avoid erroneous readings while the device is not properly seated on the body.

5) LEDs, Buzzer, and Pushbuttons

Three LEDs are placed on the side of the device body, configured in three modes: alternating mode indicating BLE advertising, blinking mode indicating that the device is turned on and is functional, and a charging mode indicating the amount of battery charge as well as a buzzer to provide audible notifications of BLE being disconnected or a misplaced microSD. In addition, two pushbuttons are placed alongside the LEDs, one to exclusively enable Bluetooth advertising for one minute (marked with a Bluetooth logo), another for turning the device as well as Bluetooth advertising on normal press and turning the device off on long press (marked with a power on/off symbol).

C. Printed Circuit Board Design

The Printed Circuit Board (PCB), which is 0.8 mm thick, was designed to accommodate high-frequency parts and the industrial standards of body design. An electroless nickel immersion gold (ENIG) surface finish was chosen for the final manufactured board to ensure RoHS compliance (Fig. 2).

D. Firmware Functionality Flowchart

The data collection timer affects the ECG data, recorded at 256 samples per second, and the accelerometer data, recorded at 50 samples per second. Every 50 ms, a check runs as to whether a central BLE and/or a microSD is connected, and data from FIFO storage on the sensors is sent accordingly. Note that only FAT32 is currently supported for microSD storage. During the time no sensor interactions occur, the device goes into sleep mode.

The ADC timer measures battery every 500ms. A resistor divider scales the battery voltage to the microcontroller voltage to send a percentage level and charging status via BLE. Also, an individual UI timer orchestrates the LEDs and the buzzer.

As discussed in the previous section, the Bluetooth pushbutton calls an interrupt to initialize Bluetooth advertising and the power button to power the device on/off. Each sensor is individually configurable via BLE through the peripheral. The discussed procedure is shown in Fig. 3.

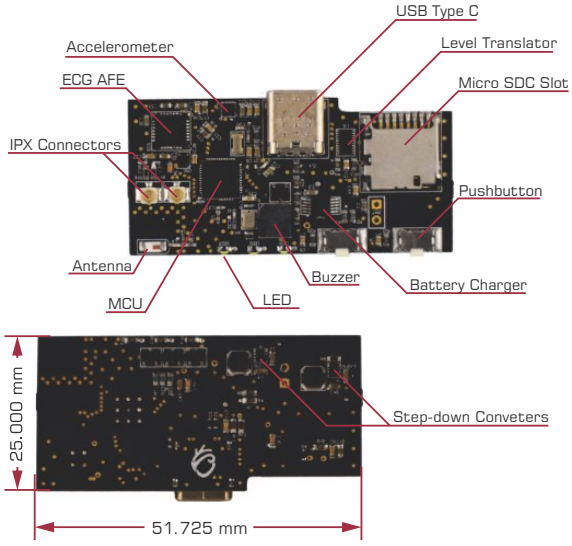

Fig. 2. Pictures from PCB top layout (top) and bottom layout (bottom). The critical parts and the PCB dimensions are marked.

E. Body Design

The body frame is 3D printed using HP Multi Jet Fusion technology, with PA12 medical grade material [23] featuring a curved ergonomic design. The intended setup is setting the device upright, which puts both electrodes on a lead near the lead II (Fig. 4). Lead II was chosen since it is more suitable for rhythm detection and gives a good view of the P wave [24]. The wings are curved in all three dimensions in two opposite directions aiming to allow unobstructed patient movement and improved signal accuracy and stability. The honeycomb design was adopted to provide more flexibility while improving the aesthetics. The outer curve of the wing conceals and protects the wiring connecting the patch to the

circuit. The stainless-steel lid in the closed state covers the micro-SD slot and the USB Type-C jack. Furthermore, it increases the physical durability of the device. The medical practitioner can slide the lid upwards in its set constraints to access the slot and the jack.

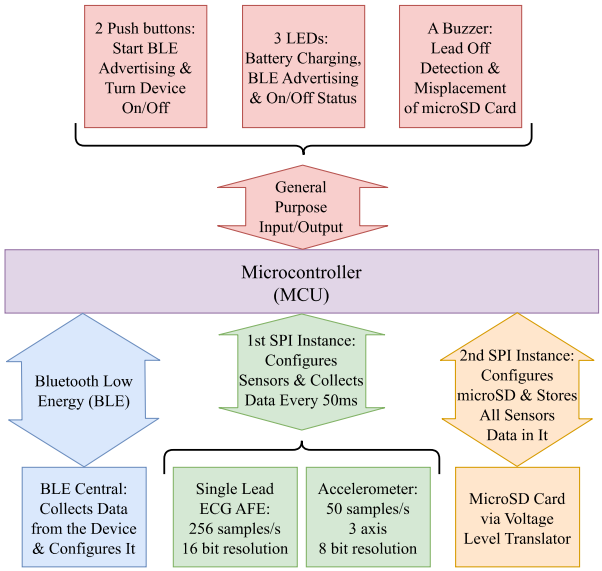

Fig. 3. Firmware flowchart. The first SPI instance takes data from the accelerometer, the second takes microSD, and the rest of the firmware deals with interface elements from MCU input/output pins and device configuration via BLE.

The HP PA12 biocompatible material has a dense and strong structure with a balanced property profile [23]. The following certifications were considered in choosing this material: USP Class I-VI, US FDA guidance for Intact Skin Surface Devices, RoHS, EU REACH, and PAHs [23]. The side view, exploded view, critical parts and dimensions of the product are demonstrated in Fig. 5, Fig. 6, Fig. 7, and Fig. 8 respectively.

Fig. 4. The device on the body (left) and a render of the device (right)

Fig. 5. A photograph of the final product

Fig. 6. A render of the exploded view of the body

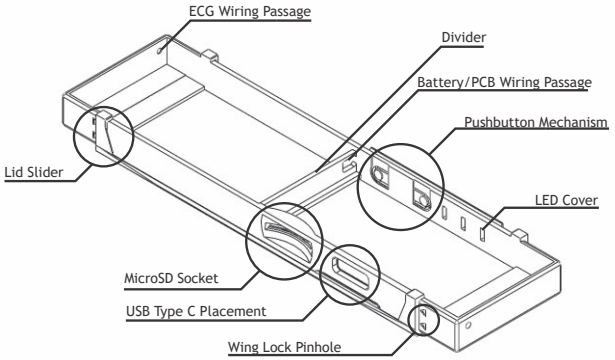

Fig. 7. Critical parts of the main enclosure

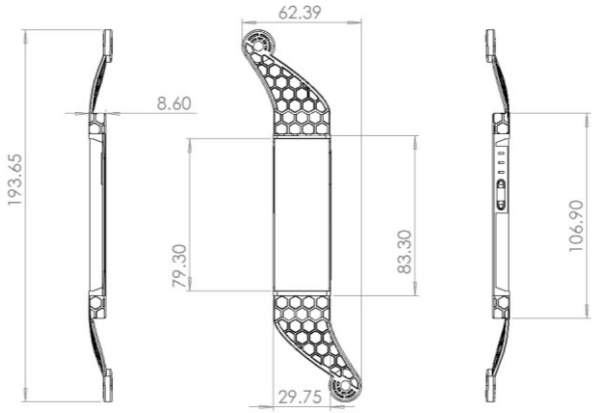

Fig. 8. Body dimensions (all dimensions in millimeters)

III. Software Design

A. Software Overview

The software introduces a comprehensive platform for ECG signal viewing and processing, implemented as an Android application and a web application via Internet of Things (IoT). Server-side processing detects features such as R-to-R intervals and arrhythmias via artificial intelligence, and the Android application serves as a real-time signal viewer.

B. Android Application and Web Application

The following section covers the parts concerning the end-users and medical practitioners using the service.

1) Web Application

A practitioner can create and modify patient profiles through a web application accessible through a web browser. All the APIs used in the Web Application, including those used for logging in, uploading data, annotating, and commenting on the signal were designed via the RESTful API. The cloud storage service was designed from scratch for this purpose. The signal analysis and arrythmia detection are only available online via the web service, but the device does not require Internet connection to record data prior to uploading on the server. It allows complete access to patient data on multiple devices (e.g. smartphones, laptops etc.). All interactions are encrypted via the SSL protocol. Spring Security was used as a means of security by only allowing access to server data to the authorized web application. The ".ECG" and ".ACC" files themselves hold no patient identity data and all ECG signals and data regarding patient information is encrypted on the server.

2) Signal Analyzer Interface

The microSD card data, alongside patient names, and sampling dates are saved on the cloud to enable viewing and

analyzing ECG data remotely. Arrhythmia detection algorithms are triggered server-side, and then the output is shown on a webpage, visually marking arrhythmia, and R-to-R intervals in milliseconds. The user can edit generated annotations, add comments on any selected signal segment and measure the interval between any two selected points in seconds. The result can be exported to a PDF file (Fig. 9).

Fig. 9. A screenshot of the web application, demonstrating the analyzer interface.

3) Android Application

The Android application was designed using the native Android SDK. After logging in, the data received through BLE is displayed in real-time and can be partially stored locally. An option to configure external devices also exists (Fig. 10). The Android application can also optionally send the sensor data to the server for analysis over WebSocket protocol, although the offline functionalities are available without an Internet connection. The JSON Web Token (JWT) method was used to ensure the security of the data transfer and to stop any unauthorized access to the server data.

Fig. 10. A screenshot of the Android application demonstrating the signal before and after filtering in dark (left) and light (right) themes.

4) Request Handling

All HTTP requests sent from the web application and the android application (e.g., login forms) are received and processed through RESTful web service and stored on the server whenever needed. In addition, all patient and practitioner data are stored on a SQL-based database (MySQL), and recorded signal files are stored individually on the server, easily accessible by the uploader through the Internet (Fig. 11).

C. Server-Side Processing

The following sector covers the server-side data analysis.

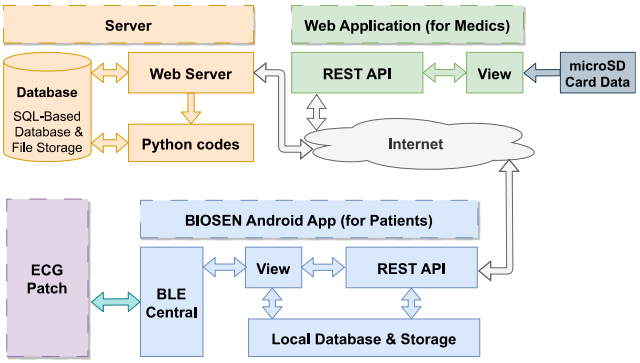

Fig. 11. The diagram of the web platform using IoT

1) Pre-Processing and Filtering

The industrial standard for modern ECG recording is a bandpass ranging from 0.5 Hz to 100 Hz or 150 Hz [25]. Baseline wandering (BW) and Power Line Interference (PLI) are two significant noise sources in ECG signals. BW is a low-frequency artifact moving the x-axis higher or lower than the intended fixed position. Patient movement, breathing, and improper electrodes can lead to BW noise. The frequency content range of BW noise is in the range of 0.5 Hz. Another primary source of noise in ECG signals is power line interference (PLI). The frequency content range of PLI is either 50 Hz or 60 Hz (based on the location) and the associated harmonics [26]. The sample rate of the ECG Patch is 256 samples per second, so its Nyquist frequency is equal to 128 Hz, which covers the frequency content of the ECG signal. Therefore, based on the frequency range of ECG signals, it can be concluded that the desired filter should pass every frequency content in the range of 0.5 Hz up to 100 Hz except for 50 Hz (or 60 Hz) in particular.

Various techniques like IIR notch filtering, FIR filtering, adaptive filtering, and filtered residue method have been proposed for ECG noise removal [27]. FIR filters were chosen for this purpose since they have finite impulse responses, which stabilizes the filter. Furthermore, they can be designed to have a linear phase and require no feedback. Also, designing an FIR filter tends to be a controlled process. The simplest method of FIR filter design is the windowing method, branching into different window types [28]. Kaiser window provides a better ripple ratio and better main lobe width characteristic than other windows [29]. Therefore, as shown in Fig. 12, in the first stage of the filter, two FIR filters with the Kaiser Windowing method were utilized in parallel to remove PLI.

Moreover, median filters are a common means in BW removal [30, 31]. Therefore, to increase the efficiency of BW removal, we used a median filter in the second stage. Thus, as shown in Fig. 13 and Fig. 14, the designed filter can remove PLI and BW simultaneously.

2) R-peak Detection

The ECG signal contains five significant peaks, known as Fiducial points, shown by letters P, Q, R, S, T [32], as seen in Fig. 15. Since the R-peak in the QRS complex is the most noticeable parameter for analyzing ECG signals, many algorithms have been proposed to detect R-peaks [33]. Some of these algorithms were examined and compared in terms of accuracy and runtime speed by running each individually on the MIT-BIH dataset. To evaluate the accuracy of each algorithm, the equation in Table I is used to calculate the duration between where an R-peak occurs (as marked in the

MIT-BIH data) from the detected R by each algorithm. We have used the NeuroKit algorithm in our server since it results in higher accuracy in lower runtime.

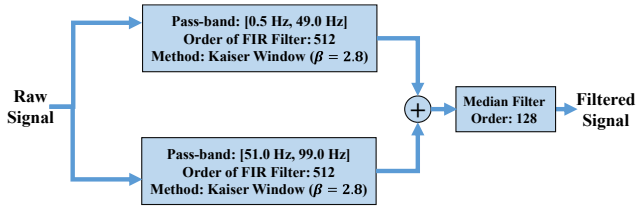

Fig. 12. Filter specifications – Initially, the signal is divided into two bands to discard the 50 Hz PLI noise and frequencies greater than 99 Hz. Subsequently, a median filter is applied to remove the baseline wander.

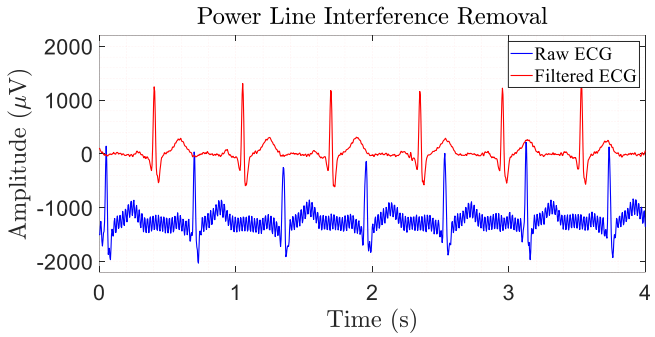

Fig. 13. PLI removal results using the proposed filter. The constant 50 Hz PLI noise is removed after the application of the filter.

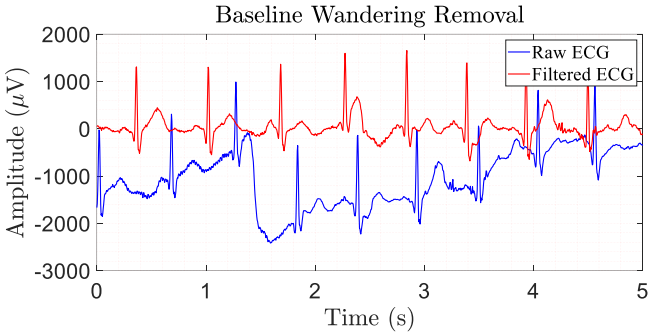

Fig. 14. BW removal results using the proposed filter. The resulting signal (red) has a fixed baseline after the application of the filter.

TABLE I

Algorithm	Runtime on a 60 min ECG signal	$\frac{\sum\lvert R_{expected} - R_{detected}\rvert}{Number\ of\ R_{expected}}$
Hamilton [34]	1.44 s	69 ms
Christov [35]	15.39 s	28 ms
Englese and Zeelenberg [36]	6.22 s	130 ms
Pan and Tompkins [37]	6.24 s	67 ms
Stationary Wavelet Transform [38]	0.75 s	59 ms
NeuroKit (slightly modified) [39]	0.13 s	15 ms

Comparison of different R-peak detection algorithms. Our modified version of the open-source NeuroKit algorithm significantly outperformed the other available methods in terms of runtime and accuracy.

3) Dataset Analysis

We use the MIT-BIH to provide an approach that can detect two significant types of arrhythmia. Unlike most prior works focused on only 2-class classification [40-45], we have examined three types of heartbeat annotation: normal, ventricular ectopic beat, and supraventricular ectopic beat. The labels 'A', 'S', 'a' and 'J' were used for supraventricular beat class, 'V' and 'E' for ventricular beat class, as well as 'N', '.', 'L', 'R', 'e' and 'j' for normal class [45, 46]. Overall, there are 98476 heartbeats which include 88462 normal, 7235 ventricular beats, and 2779 supraventricular.

4) Feature Extraction

Before feature extraction, a median filter shown in Fig. 12 is used for BW removal on each recording of the MIT-BIH dataset. We use the following segmentation method, which relies on R-peak detection, to separate every heartbeat signal, including all Fiducial points. As seen in Fig. 15, for each segment, the interval between the previous R-peak to the current is marked by $R_{n-1}R_n$. The last third of the $R_{n-1}R_n$ interval marks the beginning of each segment. The first two-thirds of the R_nR_{n+1} interval marks the end of the segment. We have extracted ten relatively quickly calculable features on each segment for different classes, which are variance of each segment to variance of corresponding recording ratio, skewness, kurtosis, RR interval, mean frequency, median frequency, OBW (frequencies occupying 99 percent of the bandwidth), band-power, previous RR interval to following RR interval ratio, and second derivative of RR interval. In addition to visual inspection with scattering features of different classes, shown in Fig. 16-a and Fig. 16-b, the Fisher score of each feature was calculated to separate effective features efficiently [47].

According to our findings on the MIT-BIH dataset, the following features tend to be more separative in classifying ventricular beats, supraventricular beats, and normal segments: second derivative of RR interval, previous RR interval to the following RR interval ratio, kurtosis, and Skewness.

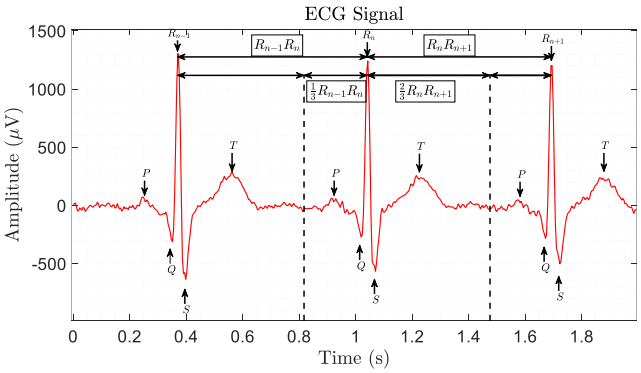

Fig. 15. A depiction of Fiducial points and segmentation selection.

5) Pattern Classification

After extracting features, artificial neural network (ANN), decision tree (DT), and K-nearest neighbor (KNN) were used for classification and compared in terms of accuracy and learning time.

a) Artificial Neural Network (ANN)

For ANN, we have used nprtool toolbox of MATLAB. The number of hidden neurons was set as 32 with 150 maximum number of iterations to avoid overfitting. All ten features were used in the process. Eighty percent of heartbeats were set as training data, and the other 20 percent were set as test data randomly. We tested three different training methods to reach higher accuracy, including Bayesian Regularization, Levenberg-Marquardt optimization, and scaled conjugate gradient. Based on our findings, Bayesian Regularization

tends to have higher accuracy than other training algorithms. The confusion matrices of ANN with the Bayesian Regularization algorithm are shown in Fig. 17.

b) Decision Tree (DT)

The maximum number of splits is set as 1024 in the Decision Tree method to avoid overfitting, equal to 1.04 percent of total heartbeats samples. Identical training and test sets were used to provide a fair comparison between DT, ANN, and KNN. Also, the same features were used in all classifiers. The confusion matrices of the Decision Tree are shown in Fig. 18.

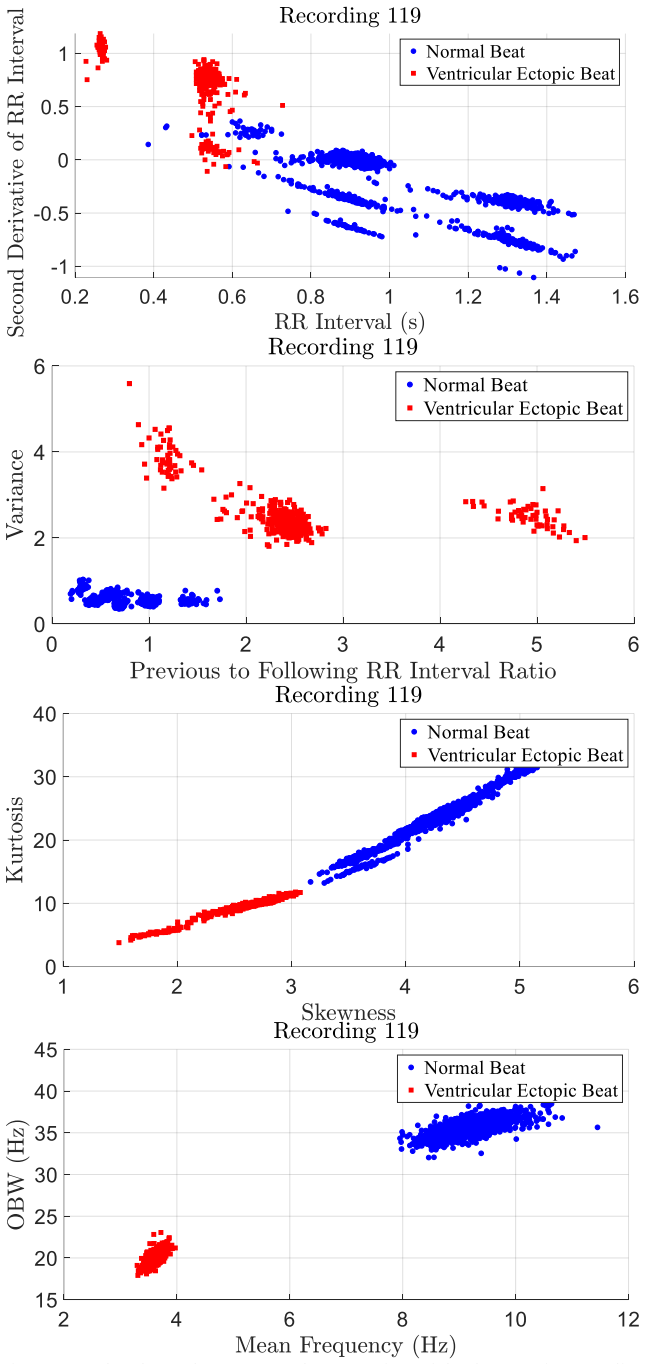

Fig. 16-a. The charts demonstrate the scattering of the features in recording 119 of MIT-BIH. As visible in the chart, the chosen criteria has a definitive separative quality.

c) K-Nearest Neighbors (KNN)

For KNN, we have used fitcknn function of MATLAB. The parameter k, which decides how many neighbors will be chosen for KNN is set as 12. In addition, the distance function is set as seuclidean. The training set, test set, and features in the three classifiers are equal. The confusion matrices of the KNN are shown in Fig. 19.

In comparing the three classifiers, although Decision Tree seems to be the fastest and the most understandable classifier, ANN and KNN yield more accurate results in test data.

6) Dataset Collection

At the time of writing this article, this section of research is being evaluated for human subject research by National Committee for Ethics in Biomedical Researches (NCEBR) Institutional Review Board (IRB). ECG and accelerometer signals will be recorded and stored from patients and healthy candidates, who sign an agreement for anonymous inclusion of the recordings in a dataset. Random excerpts of recordings are to be evaluated and annotated by a medical doctor and uploaded on https://dataset.biosengroup.com for open-source usage. The findings of personal evaluation will be compared to the findings of our AI algorithm for debugging purposes. Upon further validation of the set, we plan to expand the training of our algorithm beyond the MIT-BIH set and improve its accuracy.

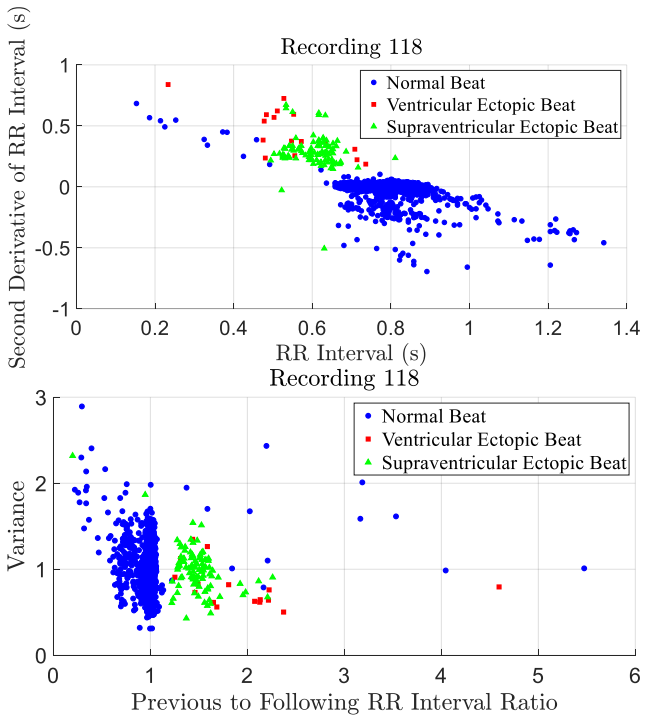

Fig. 16-b. The charts demonstrate the scattering of the features in recording 118 of MIT-BIH.

IV. Comparison with Existing Systems

This work was conceived as a research project to evolve into a commercial product. One of the primary factors was the commercial feasibility and offering enhanced connectivity and recording timeframe than the existing devices and software platforms. For this matter, we refrain from comparison with research concluded in a strictly academic environment with no large-scale commercial usage. As demonstrated in Table II, measures taken to extend the battery life appear to prolong the recording timeframe longer than the available commercial alternatives. In addition, the connectivity methods and platform availability reduce the need for third-party involvement in the analysis process.

Furthermore, signal losses occurring due to artifacts, sudden muscle movements, and device-body disconnection appears to be rare due to the flexible structure.

The main challenge of the detection section was using a 3-class system as opposed to the 2-class system commonplace in similar research while maintaining high accuracy. Table III demonstrates a comparison of various arrhythmia detection algorithms. Note that decreasing the server load required a decrease in the runtime of our algorithm. However, many similar researchers refrain from discussing runtime adequately to provide a comparison value.

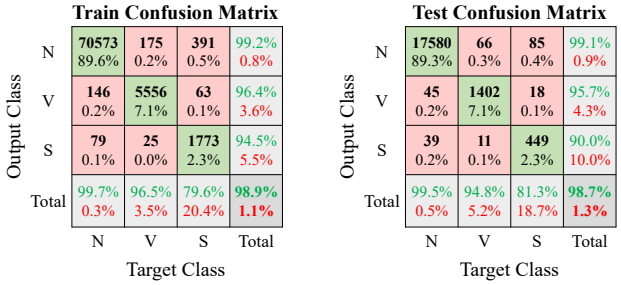

Fig. 17. ANN Train and Test Confusion Matrix ('S' stands for supraventricular ectopic beats, 'V' for ventricular ectopic beats, and 'N' for normal beats)

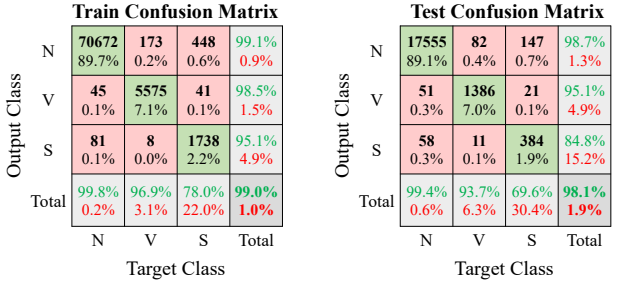

Fig. 18. DT Train and Test Confusion Matrix ('S' stands for supraventricular ectopic beats, 'V' for ventricular ectopic beats, and 'N' for normal beats)

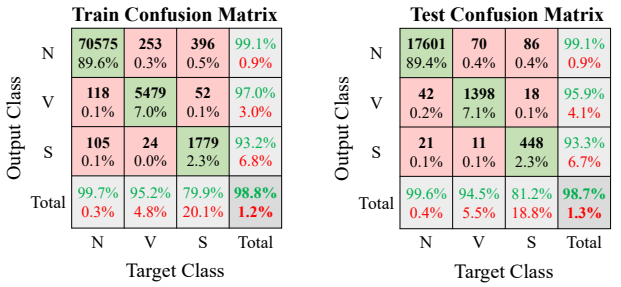

Fig. 19. KNN Train and Test Confusion Matrix ('S' stands for supraventricular ectopic beats, 'V' for ventricular ectopic beats, and 'N' for normal beats)

V. Conclusion

The hardware developed in this project shows promise as an alternative to Holter monitoring and common ECG patch devices due to better battery performance and higher resolution and sample rate. In addition, longer recording timeframes allow the detection of more sporadic arrhythmias. The general hardware design needs little to no modification as of writing. Further research might focus on powering the device with a body energy harvester for prolonged or indefinite recording periods and the use of such recordings. The new proposed ECG and accelerometer encoding format allows compression of the data and facilitates the real-time monitoring applications of the device.

Cloud-based storage allows more accessible storage and management of data than similar products. The detection algorithm shows an improvement over existing research performed on the MIT-BIH dataset and could be improved upon by integrating the collected data set into the training set. Also, further research in the software component could be performed on the usage of accelerometer data to removal noise caused by motion artifacts.

TABLE II

Device Name	Data Storage Timeframe	ECG Channel Count	ECG Resolution (bits)	ECG Sample Rate (Hz)	Data Transmission
ZIO Patch	14 days	1	10	200	Return of the device for data retrieval
SEEQ MCT	7.5 days	1	16	200	Bluetooth and cellular transmission
QardioCore	24 hours	1	16	600	Bluetooth, internal device memory
Savvy	7 days	1	16	125	Bluetooth
Generic ECG Holter Monitors	24-72 hours	3 to 12	Variable	Variable	Local download in clinic
This Work	> 14 days	1	16	256	BLE, microSD Card

A comparison of this work and commercial devices [48, 49, 50, 51].

TABLE III

Accuracy	Classifier(s)	Features	Type Detection	Ref.
92.25%	KNN, DT, Probabilistic Neural Network	8 Features	Premature Ventricular Contractions	[40]
98.90%	Learning Vector Quantization Neural Network	Lyapunov Exponent Curve	Premature Ventricular Contractions	[41]
95.40%	Multilayer Perceptron	11 features	Premature Ventricular Contractions	[42]
99.70%	KNN	Deep learning model to extract spatial features	Premature Ventricular Contractions	[43]
91.10%	Random forest	16 features	Supraventricular Tachycardia	[44]
98.7%	ANN, DT, and KNN	10 features	Ventricular and Supraventricular beats	This Work

A comparison of this project and similarly arrhythmia detection papers.

References

[1] G. A. Roth et al. "Global Burden of Cardiovascular Diseases and Risk Factors, 1990-2019: Update from the GBD 2019 Study." *Journal of the American College of Cardiology* vol. 76,25 (2020): 2982-3021. DOI: 10.1016/j.jacc.2020.11.010

[2] B.V. Reamy et al. "Prevention of Cardiovascular Disease." *Primary care* vol. 45,1 (2018): 25-44. DOI: 10.1016/j.pop.2017.11.003

[3] D. Fu. "Cardiac Arrhythmias: Diagnosis, Symptoms, and Treatments." *Cell biochemistry and biophysics* vol. 73,2 (2015): 291-296. DOI: 10.1007/s12013-015-0626-4

[4] N. Dagres et al. ": Influence of the duration of Holter monitoring on the detection of arrhythmia recurrences after catheter ablation of atrial fibrillation: implications for patient follow-up." *International journal of cardiology* vol. 139,3 (2010): 305-6. DOI: 10.1016/j.ijcard.2008.10.004

[5] J. J. Oresko et al. "A wearable smartphone-based platform for real-time

cardiovascular disease detection via electrocardiogram processing." IEEE transactions on information technology in biomedicine: a publication of the IEEE Engineering in Medicine and Biology Society vol. 14,3 (2010): 734-40. DOI: 10.1109/TITB.2010.2047865
[6] P. M. Barrett et al. "Comparison of 24-hour Holter monitoring with 14-day novel adhesive patch electrocardiographic monitoring." *The American journal of medicine* vol. 127,1 (2014): 95.e11-7. DOI: 10.1016/j.amjmed.2013.10.003
[7] Liu, Chih-Min et al. "Enhanced detection of cardiac arrhythmias utilizing 14-day continuous ECG patch monitoring." *International Journal of Cardiology* 332 (2021): 78-84 DOI: https://doi.org/10.1016/j.ijcard.2021.03.015
[8] R. Stahrenberg et al. "Enhanced detection of paroxysmal atrial fibrillation by early and prolonged continuous holter monitoring in patients with cerebral ischemia presenting in sinus rhythm." *Stroke* vol. 41,12 (2010): 2884-8. DOI: 10.1161/STROKEAHA.110.591958
[9] S. Haseeb et al. "Value of electrocardiography in coronavirus disease 2019 (COVID-19)." Journal of electrocardiology vol. 62 (2020): 39-45. DOI: 10.1016/j.jelectrocard.2020.08.007
[10] A. Pantelopoulos and N. G. Bourbakis, "A Survey on Wearable Sensor-Based Systems for Health Monitoring and Prognosis," in IEEE Transactions on Systems, Man, and Cybernetics, Part C (Applications and Reviews), vol. 40, no. 1, pp. 1-12, Jan. 2010, DOI: 10.1109/TSMCC.2009.2032660
[11] Serhani, M. A. et al(2020). ECG Monitoring Systems: Review, Architecture, Processes, and Key Challenges. *Sensors (Basel, Switzerland)*, *20*(6), 1796. https://doi.org/10.3390/s20061796
[12] G. Medic et al. "Mobile Cardiac Outpatient Telemetry Patch vs Implantable Loop Recorder in Cryptogenic Stroke Patients in the US – Cost-Minimization Model", Med Devices (Auckl), 2021;14:445-458 DOI: https://doi.org/10.2147/MDER.S337142
[13] "nRF52832 Product Specification v1.4", Nordic Semiconductor, Available: https://infocenter.nordicsemi.com/pdf/nRF52832_PS_v1.4.pdf
[14] "BQ2409x 1-A, Single-Input, Single-Cell Li-Ion and Li-Pol Battery Chargers", Texas Instruments, Available: https://www.ti.com/lit/gpn/bq24092
[15] TXB0104 4-Bit Bidirectional Voltage-Level Translator with Automatic Direction Sensing and ±15-kV ESD Protection, Texas Instruments, Available: https://www.ti.com/lit/gpn/TXB0104
[16] "Ultra-Low Power, Single-Channel Integrated Biopotential (ECG, R-to-R Detection) AFE (MAX30003)", Analog Devices (Maxim Integrated), https://datasheets.maximintegrated.com/en/ds/MAX30003.pdf
[17] "MEMS digital output motion sensor: ultra-low-power high-performance 3-axis "femto" accelerometer (LIS2DH12)", ST, Available: https://www.st.com/resource/en/datasheet/lis2dh12.pdf
[18] "TPS62840 1.8-V to 6.5-V, 750-mA, 60-nA IQ Step-Down Converter", Texas Instruments, Available: https://www.ti.com/lit/gpn/tps62840
[19] Scher, A. M., and Young A.C., "Frequency analysis of the electrocardiogram." Circulation Research 8, no. 2 (1960): 344-346.
[20] Langner Jr, P. H., Geselowitz, D. B., and Mansure, F. T, "High-frequency components in the electrocardiograms of normal subjects and of patients with coronary heart disease", American heart journal, 1961, 62(6), pg. 746-751.
[21] Flowers, N.C et al "The anatomic basis for high-frequency components in the electrocardiogram." Circulation 39, no. 4,1969 pg. 531-539.
[22] Franke, E. K., Braunstein J.R., and Zellner D.C, "Study of high frequency components in electrocardiogram by power spectrum analysis.", Circulation Research 10, no. 6, 1962 pg. 870-879.
[23] "HP 3D High Reusability PA 12 Datasheet", CimQuest, Accessed on 21/6/2021 [Online], Available: https://cimquest-inc.com/resource-center/HP/Materials/HP-PA12-Datasheet.pdf
[24] S. Meek, and F. Morris. "ABC of clinical electrocardiography. Introduction. I-Leads, rate, rhythm, and cardiac axis." *BMJ (Clinical research ed.)* vol. 324,7334 (2002): 415-8. DOI: 10.1136/bmj.324.7334.415
[25] L.G. Tereshchenko and M. E. Josephson, "Frequency content and characteristics of ventricular conduction." *Journal of electrocardiology* vol. 48,6 (2015): 933-7. DOI: 10.1016/j.jelectrocard.2015.08.034
[26] R. Kher, "Signal Processing Techniques for Removing Noise from ECG Signals." J Biomed Eng 1: 1-9., Accessed: 8/6/2021, Available: http://www.jscholaronline.org/articles/JBER/Signal-Processing.pdf
[27] A. Banerjee, M. H. Kolekar, L. and Garg, B. Chakraborty, Chapter 6 of "Internet of Things for Healthcare Technologies", Springer-Verlag, New York; Berlin, Germany; Vienna, Austria
[28] A. V. Oppenheim and R. W. Schafer, Chapter 7 of "Discrete-time Signal Processing", 3rd ed., Pearson; USA
[29] T. Kaya and M. C. Ince, "The Obtaining of Window Function Having Useful Spectral Parameters by Helping of Genetic Algorithm", Procedia - Social and Behavioral Sciences, Vol. 83, 2013, Pg. 563-568, ISSN 1877-0428. DOI: 10.1016/j.sbspro.2013.06.107
[30] A. E. Awodeyi, S. R. Alty and M. Ghavami, "Median Filter Approach for Removal of Baseline Wander in Photoplethysmography Signals," 2013 European Modelling Symposium, 2013, pp. 261-264, DOI: 10.1109/EMS.2013.45
[31] Y. Xin et al. "ECG baseline wander correction based on mean-median filter and empirical mode decomposition." *Bio-medical materials and engineering* vol. 24,1 (2014): 365-71. DOI: 10.3233/BME-130820
[32] J. Aspuru et al. "Segmentation of the ECG Signal by Means of a Linear Regression Algorithm." *Sensors (Basel, Switzerland)* vol. 19,4 775. 14 Feb. 2019, DOI: 10.3390/s19040775
[33] X. Benlian, P. et al. "R Peak Detection Method Using Wavelet Transform and Modified Shannon Energy Envelope". Journal of Healthcare Engineering. DOI: 10.1155/2017/4901017
[34] P. Hamilton, "Open-Source ECG Analysis", EP Limited, Somerville, USA, Accessed on 16/6/2021, Available: https://www.cinc.org/old/Proceedings/2002/pdf/101.pdf
[35] I.I. Christov, "Real time electrocardiogram QRS detection using combined adaptive threshold". BioMed Eng OnLine 3**,** 28 (2004). DOI: 10.1186/1475-925X-3-28
[36] Implementation of W. Engelse and C. Zeelenberg, "A single scan algorithm for QRS detection and feature extraction", IEEE Comp. in Cardiology, vol. 6, pp. 37-42, 1979 with modifications A. Lourenco, H. Silva, P. Leite, R. Lourenco and A. Fred, "Real Time Electrocardiogram Segmentation for Finger Based ECG Biometrics", BIOSIGNALS 2012, pp. 49-54, 2012. Usage
[37] J. Pan and W. J. Tompkins," A Real-Time QRS Detection Algorithm", IEEE Transactions on Biomedical Engineering, Vol. BME-32, No. 3, 1985 Available: https://www.robots.ox.ac.uk/~gari/teaching/cdt/A3/readings/ECG/Pan+Tompkins.pdf
[38] V. Kalidas and L. Tamil, "Real-time QRS detector using Stationary Wavelet Transform for Automated ECG Analysis," in *2017 IEEE 17th International Conference on Bioinformatics and Bioengineering (BIBE)*, Washington, DC, USA, 2017 pp. 457-461. DOI: 10.1109/BIBE.2017.00-12
[39] D. Makowski et al. (2021). NeuroKit2: A Python toolbox for neurophysiological signal processing. Behavior Research Methods. DOI: 10.3758/s13428-020-01516-y
[40] T.S. Hock et al. "Automated Detection of Premature Ventricular Contraction Using Recurrence Quantification Analysis on Heart Rate Signals",Journal of Medical Imaging and Health Informatics. DOI: 10.1166/jmihi.2013.1181
[41] X. Liu et al
"Automatic diagnosis of premature ventricular contraction based on Lyapunov exponents and LVQ neural network,Computer", Methods and Programs in Biomedicine, Volume 122, Issue 1, 2015, Pages 47-55, ISSN 0169-2607. DOI: 10.1016/j.cmpb.2015.06.010
[42] A. Ebrahimzadeh and A. Khazaee, "Detection of premature ventricular contractions using MLP neural networks: A comparative study", Measurement, Volume 43, Issue 1, 2010, Pages 103-112, ISSN 0263-2241. DOI: 10.1016/j.measurement. 2009.07.002.
[43] J. Yu et al. "Automatic Premature Ventricular Contraction Detection Using Deep Metric Learning and KNN." *Biosensors* vol. 11,3 69. 4 Mar. 2021, DOI: 10.3390/bios11030069
[44] Z. Li et al., "Supraventricular Tachycardia Detection via Machine Learning Algorithms," 2018 IEEE International Conference on Bioinformatics and Biomedicine (BIBM), 2018, pp. 2419-2422, DOI: 10.1109/BIBM.2018.8621164.
[45]: B. Rajoub, "Machine learning in biomedical signal processing with ECG applications", Chapter 4, Pages 91-112,
Developments in Biomedical Engineering and Bioelectronics, Biomedical Signal Processing and Artificial Intelligence in Healthcare, Academic Press, 2020, DOI: 10.1016/B978-0-12-818946-7.00004-4
[46] G. B. Moody, **"**MIT-BIH Arrhythmia Database Directory"**,** Hypertext edition, Harvard-MIT Division of Health Sciences and Technology Biomedical Engineering Center, 1997, Available: https://physionet.org/physiobank/database/html/mitdbdir/intro.htm
[47] Q. Gu, Z. Li and J. Han. (2012). Generalized Fisher Score for Feature Selection. Proceedings of the 27th Conference on Uncertainty in Artificial Intelligence, UAI 2011. Available: https://arxiv.org/ftp/arxiv/papers/1202/1202.3725.pdf
[48] E. Fung et al. "Electrocardiographic patch devices and contemporary wireless cardiac monitoring." Frontiers in physiology vol. 6 149. 27 May. 2015, DOI: 10.3389/fphys.2015.00149
[49] "QARDIOCORE Wireless ECG Monitor", Qardio, Available: https://support.getqardio.com/hc/en-us/article_attachments/360071818514/QardioCore_C100_User_Manual_ENG.pdf
[50] "User's Manual", savvy, Available: https://bodycontrolmt.cz/doc/UM-1.19.3-EN.pdf
[51] L. Poposka, M. Vavlukis, H. Pejkov, and M. Gusev, "Comparison of 24 h ECG Holter Monitoring with Real-time Long-term ECG Monitoring System using ECGalert Software and Savvy Single-Lead Patch", Open Access Maced J Med Sci, vol. 9, no. B, pp. 12–17, Jan. 2021, DOI: 10.3889/oamjms.2021.4960